# Measurement report: Sources, sinks and lifetime of $NO_{xy}$ in a sub-urban temperate forest at night

Simone T. Andersen[1], Max R. McGillen[2], Chaoyang Xue[2], Tobias Seubert[1], Patrick Dewald[1], Gunther N. T. E. Türk[1], Jan Schuladen[1], Cyrielle Denjean[3], Jean-Claude Etienne[3], Olivier Garrouste[3], Marina Jamar[4], Sergio Harb[5], Manuela Cirtog[5], Vincent Michoud[6], Mathieu Cazaunau[5], Antonin Bergé[5], Christopher Cantrell[5], Sebastien Dusanter[4], Bénédicte Picquet-Varrault[5], Alexandre Kukui[7], Abdelwahid Mellouki[2,8], Lucy J. Carpenter[9], Jos Lelieveld[1], John N. Crowley[1]

[1]Atmospheric Chemistry Department, Max-Planck-Institute for Chemistry, 55128-Mainz, Germany

[2]Institut de Combustion, Aérothermique, Réactivité Environnement (ICARE), CNRS, 1C Avenue de la Recherche Scientifique, CEDEX 2, 45071 Orléans, France

[3]CNRM, Universite de Toulouse, Meteo-France, CNRS, Toulouse, France

[4]IMT Nord Europe, Institut Mines-Télécom, Université de Lille, Center for Energy and Environment, 59000 Lille, France

[5]Univ Paris Est Creteil and Université de Paris Cité, CNRS, LISA, F-94010 Créteil, France

[6]Université Paris Cité and Univ Paris Est Creteil, CNRS, LISA, F-75013 Paris, France

[7]Laboratoire de Physique et Chimie de l'Environnement et de l'Espace (LPC2E), CNRS Orléans, France

[8]University Mohammed VI Polytechnic (UM6P), Lot 660, Hay Moulay Rachid Ben Guerir, 43150, Morocco

[9]Wolfson Atmospheric Chemistry Laboratory, Department of Chemistry, University of York, York, UK

*Correspondence to*: Simone T. Andersen (simone.andersen@mpic.de) and John N. Crowley (john.crowley@mpic.de)

## 1 Abstract

The budget of reactive nitrogen species, which play a central role in atmospheric chemistry (e.g. in photochemical $O_3$ production), is poorly understood in forested regions. In this study, ~~T~~through observations of NO, $NO_2$, $NO_{~~y~~}$ and $O_3$ in the Rambouillet forest near Paris, France, ~~(as part of the ACROSS campaign, 2022)~~ we have examined~~gained insight into~~ nighttime processes controlling $NO_{~~x~~}$ in an anthropogenically impacted forest environment. $O_3$ mixing ratios displayed a strong diel profile at the site, which was driven by a variable but generally rapid deposition to soil and foliar surfaces. The $O_3$ diel profile was strongly influenced by relative humidity~~, which impacted the surface resistance to uptake,~~ and temperature inversion~~, which influenced the rate of entrainment of $O_3$ from above the canopy~~. Only when the $O_3$ mixing ratio was sufficiently low (and thus the NO lifetime sufficiently long), were sustained NO peaks observed above the instrumental detection limit, enabling derivation of average NO emission rates from the soil of ~1.4 ppbv $h^{-1}$. Observations of the lack of increase in $NO_2$ at night, despite a significant production rate from the reaction of NO with $O_3$, enabled an effective lifetime of $NO_2$ of ~0.5-3 h to be derived. As the loss of $NO_2$ was not compensated by the formation of gas- or particle-phase reactive nitrogen species it was presumably driven by deposition to soil and foliar surfaces, or any products formed were themselves short-lived with respect to deposition. By comparison, the daytime lifetime of $NO_2$ with respect to loss by reaction with OH is about 1 day. Our results indicate~~We conclude~~ that the nighttime deposition of $NO_2$ is a major sink of boundary layer $NO_{~~x~~}$ in this temperate forest environment.

## 2 Introduction

Nitrogen oxides ($NO_{~~x~~}$ = NO + $NO_2$) are pollutant trace gases, which play a key role in the atmosphere by producing or destroying tropospheric ozone ($O_3$), which can cause respiratory illness (Ciencewicki and Jaspers, 2007) and damage to plants (Emberson et al., 2018). Photolysis of nitrogen dioxide ($NO_2$) (R1) is the primary source of tropospheric ozone ($O_3$), and the nitric oxide (NO) product is oxidized back to $NO_2$ either by $O_3$ (R2) or by organic peroxy radicals ($RO_2$, under formation of alkoxy radicals (RO)) or hydroperoxyl radicals ($HO_2$) (R3, R4) (Lightfoot et al., 1992). The latter results in formation of the hydroxyl radical (OH) radical, and R3 and R4 thus represent routes to recycle the most important atmospheric radical initiator of oxidation (Hens et al., 2014). It is, therefore, essential to understand the sources and sinks of $NO_{~~x~~}$ in the atmosphere.

$$NO_2 + h\nu\ (+O_2) \rightarrow NO + O_3 \quad \text{(R1)}$$

$$NO + O_3 \rightarrow NO_2 + O_2 \quad \text{(R2)}$$

$$NO + RO_2 \rightarrow NO_2 + RO \quad \text{(R3)}$$

$$NO + HO_2 \rightarrow NO_2 + OH \quad \text{(R4)}$$

The dominant global sources of $NO_{x}$ are anthropogenic in the form of combustion of fossil fuels and to a lesser degree biomass burning and agricultural soils. The natural sources, which include lightning (Schumann and Huntrieser, 2007), wildfires (Val Martin et al., 2008), and unperturbed soil emissions from microbial activities (Davidson and Kingerlee, 1997), are important in regions remote from anthropogenic sources. $NO_2$ and NO both react with peroxy radicals in the atmosphere to produce organic nitrates (R5-R6), including peroxy nitrates ($RO_2NO_2$) and alkyl nitrates ($RONO_2$), which are important precursors for the formation of secondary organic aerosols (SOA) (Hallquist et al., 2009; Kanakidou et al., 2005; Kiendler-Scharr et al., 2016). $NO_2$ also reacts with OH radicals, $O_3$ and nitrate radicals ($NO_3$) to form nitric acid ($HNO_3$) (R7), $NO_3$ radicals (R8), and dinitrogen pentoxide ($N_2O_5$) (R9), respectively. $N_2O_5$ is in thermal equilibrium with $NO_2$ and $NO_3$ and can interact with aqueous aerosol or moist surfaces to form $HNO_3$ (R10) (Kane et al., 2001) or nitryl chloride ($ClNO_2$) (Phillips et al., 2013; Phillips et al., 2012). Organic nitrates, SOA, and $HNO_3$ are all removed from the boundary layer through dry and wet deposition which thereby removes $NO_{x}$ from the atmosphere.

$$NO_2 + RO_2 + M \rightarrow RO_2NO_2 + M \quad \text{(R5)}$$

$$NO + RO_2 + M \rightarrow RONO_2 + M \quad \text{(R6)}$$

$$NO_2 + OH + M \rightarrow HNO_3 + M \quad \text{(R7)}$$

$$NO_2 + O_3 \rightarrow NO_3 + O_2 \quad \text{(R8)}$$

$$NO_2 + NO_3 + M \rightleftharpoons N_2O_5 + M \quad \text{(R9)}$$

$$N_2O_5 + H_2O\,(aq) \rightarrow 2\,HNO_3\,(aq) \quad \text{(R10)}$$

In the planetary boundary layer, $NO_2$ is also lost through dry deposition to surfaces such as soil and leaves. Deposition takes places both at nighttime and daytime, but is expected to be more efficient during daytime due to increased mixing through turbulence. When $NO_2$ deposits onto humid surfaces, it can lead to the production of nitrous acid (HONO), which can be released to the atmosphere (Meusel et al., 2016; Elshorbany et al., 2012). $NO_2$ uptake on leaves takes place through stomatal and non-stomatal processes, which have been reported to depend on multiple factors such as stomata aperture and relative humidity. Stomatal uptake primarily occurs at daytime when the stomata are open, leading to increased $NO_2$ loss compared to nighttime, when the stomata are not fully open (Delaria et al., 2020; Delaria et al., 2018; Chaparro-Suarez et al., 2011). Non-stomatal uptake occurs through the cuticles, though the importance of cuticular uptake has been reported to be small compared to the stomatal uptake (Delaria and Cohen, 2020; Delaria et al., 2020). $NO_2$ uptake to leaves is reported to be enhanced in the presence of water films, which may exist when the relative humidity is >70% (Thoene et al., 1996; Weber and Rennenberg, 1996; Burkhardt and Eiden, 1994). There is, however, no consensus on this process, as other studies have not observed this effect (Gessler et al., 2000). Most recent work shows that the interactions with foliar surfaces is uni-directional, i.e. emissions are negligible (Delaria et al., 2020).

At nighttime, $NO_2$ photolysis ceases and as a consequence, in the absence of combustion sources, the main sources of NO are emissions from soils (Jaeglé et al., 2005). Since NO is oxidised efficiently by $O_3$ at night, its concentration will be highest at the surface and will decrease with altitude. The vertical profile of $O_3$ is the opposite owing to its physical loss due to deposition near the surface and through chemical reaction with NO and/or alkenes combined with entrainment from the nocturnal residual layer. As $NO_2$ is produced from the reaction between NO and $O_3$, its vertical gradient is expected to be weaker than those of NO and $O_3$ (Geyer and Stutz, 2004; Stutz et al., 2004).

In this study we use measurements from the ACROSS (Atmospheric ChemistRy Of the Suburban foreSt) campaign to investigate the nighttime sources and sinks of $NO_{x}$ in a temperate forest. $O_3$ measurements are used to explain the observed NO features and measurements of $NO_2$ and total gas-phase nitrogen species ($NO_{y}$) and particulate nitrate are used to investigate the lifetime and fate of $NO_{x}$ in the forest environment.

## 3 The ACROSS Campaign

The ACROSS campaign (13th of June 2022 to 25th of July 2022) was conducted in multiple locations in and around Paris, France (Cantrell and Michoud, 2022). Here we present measurements from the Rambouillet forest supersite located approximately 50 km southwest of Paris (48.687, 1.704). The forest consists of approximately 70% oak, 20% pine, and small contributions from beech and chestnut. The top of the forest canopy around the supersite was around 20-25 m. Several instrumented containers were placed in a clearing (~697 $m^2$) together with a 41 m measurement tower. Most of the instruments used in this study were located in two different containers (MPIC and Orléans). The sampling inlets of the two containers were approximately 17 m apart and the tower was approximately 9 m from the MPIC container and 16 m from the Orléans container. The soil measurements were carried out at the bottom of the tower, approximately 13 m from the MPIC container and approximately 17 m from the Orleans container. All the instruments used in this study are described briefly below.

### 3.1 Measurements

#### 3.1.1 Ground

$NO_2$ was measured using two different cavity ringdown spectroscopy (CRDS) instruments with co-located inlets sampling from a high-volume-flow stainless steel tube (10 $m^3$ $min^{-1}$; 15 cm diameter, 0.2 s residence time) taking air from a height of 5.4 m above ground. One of the instruments (5CH-CRDS) consists of 3 cavities operated at 408 nm to measure $NO_2$ and, via their thermal dissociation to $NO_2$, total peroxy nitrates (∑PNs, 448 K) and total alkyl nitrates (∑ANs, 648 K). Two additional cavities, operated at 662 nm, measured $NO_3$ and (via thermal dissociation to $NO_3$, 373 K) $N_2O_5$ (Sobanski et al., 2016). During this campaign, the $NO_2$ cavity had a limit of detection (LOD) of 9.7 pptv for 1 min averaging (3σ). The second instrument (k-NO3) primarily

measures the $NO_3$ reactivity, but also has a cavity operated at 405 nm for the measurement of $NO_2$ (Liebmann et al., 2018).

Another CRDS instrument was used to measure $NO_{x}$, $NO_{y}$, and particulate nitrate ($pNO_3$) from co-located inlets near the high-volume-flow stainless steel tube. $NO_{x}$ was measured by adding $O_3$ to the ambient sample, thereby oxidizing NO to $NO_2$, which was measured with CRDS at 405 nm (Friedrich et al., 2020). A judicious choice of $O_3$ and reaction time ensured that minimal (>1%) of $NO_2$ was oxidized to $NO_3$. At times with low (or zero) NO, $NO_{x}$ concentrations were in close agreement with both $NO_2$ measurements. $NO_{y}$ was measured by passing ambient air through a quartz inlet at ~ 900 K which quantitatively converts reactive nitrogen trace-gases to NO or $NO_2$. Exceptions are $N_2O$, HCN and $NH_3$, which are not detected. In this location, $NO_{y}$ is expected to consist mainly of $NO_{x}$ + $NO_3$ + $N_2O_5$ + $HNO_3$ + PNs + ANs + HONO + $ClNO_2$ + particulate nitrates ($pNO_3$).

Particulate nitrates (both organic and inorganic) were separately measured (as $NO_{y}$) after denuding gas-phase reactive nitrogen species (Friedrich et al., 2020). To achieve this, problems involving the ineffective trapping of gas-phase $NO_{x}$ by the denuder was eliminated, as will be described in a forthcoming technical paper.

$O_3$ was measured from the high-volume-flow stainless-steel tube with a commercial instrument (2B Technologies model 205) using UV absorption at 254 nm. The LOD is 2 ppbv for 10 s averaging time.

A spectral radiometer (metcon Gmbh) was installed near the co-located inlets on top of the MPIC container to measure actinic fluxes, which were used to calculate photolysis frequencies as described elsewhere (Meusel et al., 2016).

NO was measured from the Orléans container using a commercial chemiluminescence instrument (Ecophysics CLD 780 TR, henceforth CLD) with an LOD of 10 pptv for 1 min averaging time. The sampling height for NO measurements was about 0.6 and 3.2 m above the container top and the ground surface, respectively. The NO measurements required correction due to a change in the CLD sensitivity during the campaign caused by an interruption in the instrument's oxygen supply. The corrections and the corrective procedure are described in the SI.

HONO was measured by a commercial long-path absorption photometer (LOPAP-03, QUMA GmbH, Germany) with a sampling height of 2.0 m above the ground level. Details about the LOPAP instrument can be found elsewhere (Heland et al., 2001; Kleffmann et al., 2006). During the campaign, the LOPAP was calibrated by diluted nitrite when changing any supporting solutions. Zero calibration by measuring synthetic air was conducted 2-3 times per day. The detection limit is < 5 pptv.

The sum of peroxy radicals, $XO_2$=$HO_2$+$RO_2$, was measured by their conversion to $H_2SO_4$ in presence of NO and $SO_2$ and detection of the generated $H_2SO_4$ using $NO_3^-$ CIMS (Kukui et al., 2008). The calibration coefficient is determined using $N_2O$ actinometry and OH/$RO_2$ generation

in a turbulent flow reactor by photolysis of $N_2O$ or $H_2O$ at 184.9 nm. The calibration of $HO_2$, $CH_3O_2$ and other $RO_2$ is performed by adding into the calibration reactor CO, $CH_4$ (or other $RO_2$ precursors) converting OH to $RO_2$. The overall estimated calibration accuracy ($2\sigma$) for $XO_2$ is about 30%, although the uncertainty of the $XO_2$ measurements is typically higher due to uncertainty in ambient air $XO_2$ composition. The lower limit of detection for $XO_2$ radicals at S/N=3 and a 4 minute integration time is $2\times10^6$ molecule $cm^{-3}$.

Time series of the most relevant measurements can be found in Figure S1-2. Due to missing total $NO_{~~x}$ and $NO_{~~y}$ measurements prior to June 25th and NO after July 18th, the data analysis is focused on the time period in between these dates.

### 3.1.2 Tower

Measurements at 41 m were conducted with instruments located on the tower as well as through a manifold with an inlet at the top of the tower. The manifold was built from glass tubing (4.9 cm inner diameter, Borodrain) with a residence time in the manifold of 2.1 s. $NO_2$ was measured using a cavity attenuated phase shift (CAPS) instrument on the tower with an LOD of 40 pptv, which was zeroed every 1-2 hours. NO and $O_3$ were both measured from the manifold using a chemiluminescence instrument with a LOD of 30 pptv and a HORIBA (APOA370) with an LOD of 2.5 ppbv, respectively. The NO measurements were corrected for losses due to the reaction of NO with $O_3$ in the manifold and the sampling line (total 5.5 s), with corrections ranging from 1-28%. Time series of all three measurements are plotted in Figure S3.

### 3.1.3 Meteorology and Soil

Ambient temperature was measured at four different heights on the tower; 5 m, 13 m, 21 m, and 41 m using temperature sensors from Atexis (PT1000) and Thermoest (PT100). Relative humidity was measured at 5 m using a Vaisala humidity sensor (HMP45A). Soil temperature and moisture were measured at 5 cm, 10 cm, and 30 cm below the surface using probes from Thermoest (PT100) and Delta T (Thetaprobe ML2X), respectively. Wind speed and direction were measured at 41 m using a wind monitor from Young Company. Time series of all the meteorological and soil measurements are shown in Figure S4-5.

## 3.2 HYSPLIT

To identify different air masses, 48-hour back trajectories were simulated every hour at a terminating height of 40 m using the Hybrid Single-Particle Lagrangian Integrated Trajectory model (HYSPLIT, version 4, 2019) (Draxler and Rolph, 2011). The back-trajectories were modelled using meteorological data from the Global Data Assimilation System (GDAS) at a resolution of 1 degree. This led to the separation of the data into two periods, 25th of June to 2nd of July and 3rd of July to 18th of July, which are plotted in Figure 1. The first phase is dominated by clean air from over the Atlantic Ocean (henceforth called “Atlantic”). Back trajectories indicated that the vast majority of air masses were transported within the boundary layer prior to reaching

the site and thus may have reasonably fresh "marine influence". The second phase is dominated by air that has passed over urban locations including Paris, Brussels and the Ruhr area within the last 48 hours (henceforth called "Continental").

## 4 Results and Discussion

Two 24-hour periods of temperature (at 4 different heights), NO, $O_3$, relative humidity (RH), $NO_2$, and $NO_2$ photolysis rate constant ($JNO_2$) are plotted in Figure 2. The left panels show 24 hours with Atlantic air and the right panels 24 hours with continental air. Immediately apparent in these datasets (and in Fig S1) is the large diel cycle in $O_3$ mixing ratios, with net daytime production resulting in mid-afternoon mixing ratios between ~30 and 90 ppbv. In contrast, very low $O_3$ mixing ratios (often approaching zero) were observed at nighttime.

In the lowermost panels ($JNO_2$ measurements), the nighttime is shown in dark grey and the two light grey areas show the time before sunset (about 5 hours) and after sunrise (about 4.5 hours) when very little direct sunlight reaches the ground of the site due to shading by the trees. This leaves about 6.5 hours centred around midday when direct sunlight reaches the ground. The shading results in radiative cooling of the ground in the late afternoon and associated temperature inversions begin to form prior to sunset as can be observed in the right panels of Figure 2 and in more detail in Figure S6. The temperature inversions begin approximately at the same time as the ground temperature at 5 cm below the surface starts to decrease (see Figure S6). These conditions of insolation were relatively consistent throughout the campaign.

Clear temperature inversions were observed for both nights shown in Figure 2, the beginning and end of which are indicated by dashed lines. Vertical mixing can be reduced significantly during a temperature inversion, which is apparent from the $O_3$ and RH measurements in the right-hand panel. In both examples, $O_3$ decreases at the ground level (5.4 m) at the beginning of the temperature inversion and increases as the inversion breaks down in the morning. This behaviour is understood in terms of $O_3$ loss to soil surfaces and through stomatal and non-stomatal uptake on leaves (Zhou et al., 2017; Rannik et al., 2012; Altimir et al., 2006; Ganzeveld and Lelieveld, 1995) as well as through chemical reactions with e.g. NO, $NO_2$ and unsaturated (biogenic) organics (Kurpius and Goldstein, 2003). Reduced vertical mixing means that during the inversion, $O_3$ is only slowly replenished by downward mixing of air masses above the canopy where higher $O_3$ levels are observed. In contrast, the RH behaves in the opposite sense as the air above the inversion is drier than close to the ground, where evapotranspiration contributes to enhanced water vapour concentrations.

If the only source of NO was the photolysis of $NO_2$, NO mixing ratios would be expected to follow the $NO_2$ photolysis rate during the day and tend to zero at night as NO is oxidized on a time scale of minutes (for $O_3$ > 10 ppb) to $NO_2$ by $O_3$. This was not always the case during ACROSS. A pronounced NO peak (up to ~2 ppbv) was observed at ground level between 00:00 and 06:00 UTC (02:00 and 08:00 local time) during the phase dominated by Atlantic air, shown in Figure 2, which is absent in the phase dominated by continental air. The peak occurs prior to sunrise and is only observed by the ground-level measurements suggesting a non-photolytic source of NO close to the

ground, which is discussed further below. Very low (0-5 ppbv) $O_3$ mixing ratios coincide with the sustained nighttime NO peak observed, which is never reached in the example from the continental phase, although in both cases clear temperature inversions were seen. Additional examples of sustained NO peaks (i.e. lasting several hours at level between 1 and 2 ppbv) at night during the first phase are shown in Figure S7. Examples of additional nights with temperature inversions during phase 2, where NO mixing ratios remained close to zero, are shown in Figure S8.

### 4.1 Nighttime Ozone Loss

For each night between June 17th and July 22nd the net $O_3$ loss rate constant, $k_L(O_3)$ was derived by fitting exponential expressions to the data for periods of 4.5 to 8 hours. $k_L(O_3)$ was highly variable, with values between $1.8 \times 10^{-5}$ $s^{-1}$ and $3.0 \times 10^{-4}$ $s^{-1}$, depending on the strength of the temperature inversion and the relative humidity (see discussion below). These values of $k_L(O_3)$ correspond to lifetimes of 1-15 hours for $O_3$ at nighttime. Chemical losses of $O_3$ occur through reactions with NO, $NO_2$, and unsaturated BVOCs (Zhou et al., 2017). Rate coefficients of reactions of $O_3$ with NO ($1.9 \times 10^{-14}$ $cm^3$ $molecule^{-1}$ $s^{-1}$ at 298 K), $NO_2$ ($3.5 \times 10^{-17}$ $cm^3$ $molecule^{-1}$ $s^{-1}$ at 298 K), limonene (a reactive terpene, $2.2 \times 10^{-16}$ $cm^3$ $molecule^{-1}$ $s^{-1}$ at 298 K), β-caryophyllene (sesquiterpene, $1.2 \times 10^{-14}$ $cm^3$ $molecule^{-1}$ $s^{-1}$ at 298 K) are low such that mixing ratios in excess of 1 ppbv for NO and β-caryophyllene would be required to explain the $O_3$ loss rate constant (IUPAC, 2024). Required mixing ratios of terpenes or $NO_2$ would be even larger (60-300 ppbv). As such high mixing ratios of NO and $NO_2$ were not observed continuously and such levels of BVOC are unlikely, we assume that chemical losses of $O_3$ are insignificant compared to deposition as previously observed (Zhou et al., 2017). Ignoring entrainment from other heights, we can then equate $k_L(O_3)$ to $(2V_d/h)$, where $V_d$ is the deposition velocity and $h$ is the boundary layer height; the factor 2 is used to account for a positive vertical gradient (Shepson et al., 1992). Using a boundary layer height of 20 m (arbitrarily set equal to the top of the canopy) gives net deposition velocities varying between 0.018 and 0.3 cm $s^{-1}$. These values for $V_d$ are in broad agreement with other studies in temperate forests, where deposition velocities for $O_3$ at nighttime have been reported to be around 0.07-0.3 cm $s^{-1}$ (Padro, 1996, 1993; Finkelstein et al., 2000; Wu et al., 2016).

In Figure 3 the $O_3$ production rate ($JNO_2 \times [NO_2]$), RH, temperature at 4 different heights and $O_3$ mixing ratio have been plotted for two nights with high average RH to illustrate the impact of temperature inversions on the net $O_3$ loss-rate constants. The production rate of $O_3$ is used to identify periods in which production is negligible. In the left panel a night without a temperature inversion is plotted, where the average RH for the period used to fit the exponential decay is 93 ± 3 %. These conditions resulted in a net $O_3$ loss-rate constant of $6.0 \times 10^{-5}$ $s^{-1}$. In contrast, the night depicted in the right panel has the same average RH (92 ± 3 %) and a very clear temperature inversion, which gives a net $O_3$ loss-rate constant of $3.0 \times 10^{-4}$ $s^{-1}$. This gives a factor of 5 between these two net $O_3$ loss-rate constants depending on whether a temperature inversion is observed or not. This can be understood in terms of the $O_3$ being replenished from above when there is no (or a weak) inversion, which is not the case when there is an inversion. Bearing this in mind, the use of $k_L(O_3)$ (a *net* $O_3$ loss constant) must result in a lower limit to $V_d$ unless strong temperature inversions (preventing $O_3$ entrainment from above) are present. The $O_3$ loss rate will also be

enhanced under conditions of strong inversion if trace-gases that are reacive towards $O_3$ are released into a very shallow boundary layer. However, as indicated above, chemical losses are not expected to compete with physical losses.

To investigate the impact of RH on the net $O_3$ loss-rate constants, two nights with temperature inversions are plotted in Figure S9; one with high RH (92 ± 3 %) and one with a lower RH (63 ± 6 %). Here we see a large decrease in $k_L(O_3)$ from $3.0 \times 10^{-4}$ $s^{-1}$ to $4.5 \times 10^{-5}$ $s^{-1}$, when going from high to lower RH. The individually determined $O_3$ loss-rate constants are plotted as a function of RH in Figure 4 and coloured depending on whether a temperature inversion is observed or not during the time period which was used for the exponential decay fit. A clear increase in $O_3$ loss-rate constants can be observed when RH increases above 70-80% when a temperature inversion was observed. A small increase at RH higher than 70-80% was also observed when temperature inversions were absent. The observed dependence of $k_L(O_3)$ on relative humidity is consistent with previous studies in forested regions, which have reported an increase in $O_3$ loss above 60-70% RH (Altimir et al., 2006; Rannik et al., 2012; Zhou et al., 2017). Altimir et al. (2006) suggested an enhancement factor which is humidity dependent above 70% RH; 1 at 70% RH, 2 at 85% RH and a sharp increase to over 5 when moving towards 100% RH. In a boreal forest these observations have been explained by the formation of a "wet skin" on leaves which enhances surface $O_3$ losses by modifying (reducing) the surface-resistance to uptake (Zhou et al., 2017). This is in broad agreement with our observations during nights with a temperature inversion (see Figure 4), and the discrepancies between the studies could be explained e.g. by different tree types, the height of the boundary layer, strength of the inversion and temperature.

The faster net rate of $O_3$ loss on nights with high relative humidity and well-defined temperature inversions explain the differences observed in the $O_3$ mixing ratios at night during the Atlantic and continental phases. The average nighttime (20:00-04:00 UTC) RH for the Atlantic phase was 87.4 ± 7.6 (1σ) % compared to 68.4 ± 12.7 (1σ) % for the continental phase, indicating that on nights with temperature inversions higher loss-rate constants would be expected for the Atlantic phase. The high RH combined with the significantly lower average peak $O_3$ mixing ratio in the Atlantic phase (34.5 ± 6.0 (1σ) ppbv between 14:00-15:00 UTC) compared to the continental phase (52.7 ± 13.6 (1σ) ppbv between 14:00-15:00 UTC) explains why on nights with temperature inversions during the Atlantic phase the $O_3$ was essentially completely depleted as shown in Figure 2 and S7.

### 4.2 Nitrogen Oxide Soil Emissions

Figure 2 (left panel) and S7 show nighttime periods in which NO was observed when $O_3$ was depleted during the Atlantic phase. The several hours duration of the period when NO was above the LOD excludes very local combustion as the source, leaving soil emissions resulting from microbial activity (Davidson and Kingerlee, 1997) as the most likely source of NO. At 293 K and 2 ppbv of $O_3$, the lifetime of NO towards reaction with $O_3$ is around 20 minutes. It is therefore reasonable to assume that NO is close to steady-state when there is 2 ppbv or more of $O_3$ available. The NO emission rate ($E_{NO}$) can therefore be equated to the loss rate of NO as described in equation (1) assuming all peroxy radicals ($XO_2$) react with the same rate coefficient as $HO_2$:

$$E_{NO} = k_{NO+O3}[NO][O_3] + k_{NO+HO2}[XO_2][NO] \quad (1)$$

where $k_{NO+O3}$ and $k_{NO+HO2}$ are the temperature-dependent rate constants for the reaction between NO and $O_3$ and $HO_2$, respectively, (IUPAC, 2024) and [NO], [$O_3$] and [$XO_2$] are the measured concentrations of NO, $O_3$ and $XO_2$, respectively. In Figure 5, NO and $E_{NO}$ (when $O_3$ > 2 ppbv) at nighttime ($JNO_2 < 10^{-5}$ $s^{-1}$) are separated by air masses and plotted against $O_3$, where the outliers are defined as being outside 1.5 × interquartile range (IQR). While the nighttime NO mixing ratio increased rapidly when $O_3$ tended towards 0 ppbv during the Atlantic phase, $O_3$ was never depleted to less than 5 ppbv during the Continental phase and therefore no sustained periods of enhanced NO were observed at nighttime. In contrast, no significant trend is found when plotting $E_{NO}$ against $O_3$ for either of the phases, which shows that the calculated soil emission of NO is not dependent on $O_3$. This indicates that while the soil is an important but variable source of NO, sustained nighttime NO peaks are only observed above the instrument LOD when $O_3$ is almost totally depleted so that the lifetime of NO is long enough to allow its concentration to build-up sufficiently.

Water content and temperature have previously been shown to impact the emission rate of NO from soil (Pilegaard, 2013; Rosenkranz et al., 2006). Rosenkranz et al. (2006) found a positive correlation between soil moisture and NO emission up to 40% water-filled pore space (WFPS) and an optimum between 12.5 and 15 °C soil temperature in a sessile oak forest in Hungary. In Figure 6, NO and $E_{NO}$ are plotted against the soil temperature and moisture at 5 cm below the surface. The measured NO mixing ratios peak towards the highest soil moisture and lowest soil temperature measured during this campaign, however, as with $O_3$, there is no significant trend in the NO emission rates with soil moisture. At the low (11.5-12.5 °C) and high (19.5-20.5 °C) nighttime soil temperatures very few measurements were made (around 2 hours combined) compared to the rest of the temperature intervals. Across the remaining temperature intervals, no significant trend was observed in the estimated NO emission.

The average NO emission rate derived for the two phases is identical with values of 1.45 ± 1.61 ppbv $h^{-1}$ (1σ, median = 1.27 ppbv $h^{-1}$) and 1.42 ± 5.68 ppbv $h^{-1}$ (1σ, median = 0.71 ppbv $h^{-1}$) for the Atlantic and Continental phases, respectively, when using data where $O_3$ > 2 ppbv. The Continental phase show much higher variability resulting from more spikes in the data during that period. When $O_3$ is completely depleted during the Atlantic phase, the increase in NO per hour results in NO emission rates of 0.3-1.8 ppbv $h^{-1}$, which is in reasonable agreement with the averages across each of the two phases when there is still $O_3$ present. By assuming a mixed nocturnal boundary layer (NBL) with a height of 20 m (top of the canopy), the average emission rates can be converted to NO emission fluxes of 16.6 ± 18.5 (1σ) and 16.2 ± 65.0 (1σ) μg N $m^{-2}$ $h^{-1}$, respectively. These values are within the range of previous measurements in different European forests with similar tree types to those found in the Rambouillet forest (see Table 1). The measurements by Pilegaard et al. (2006) and Rosenkranz et al. (2006) were all performed using the chamber technique, whereas Schindlbacher et al. (2004) measured the emission from soil samples collected in the field and exposed to different temperatures and humidity in the laboratory. The chamber-derived emission rates are all either lower or, within combined uncertainties, equal to the values determined in this study, while emission rates from the soil samples were higher than

(or, within combined uncertainties, equal to) the values derived in the present study. Davidson and Kingerlee (1997) modelled the global NO emission inventory from soil depending on the biome (e.g. temperate forest, agriculture, and savanna), and split the temperate forest category into regions affected by nitrogen deposition or not. For temperate forests not affected by nitrogen deposition, those authors estimated a flux of 0.0-0.2 kg N $ha^{-1}$ $yr^{-1}$ (0.0-2.3 μg N $m^{-2}$ $h^{-1}$), which is in good agreement with the lower measurements by Pilegaard et al. (2006). In contrast, the temperate forests impacted by nitrogen deposition had estimated fluxes of 1.1-5.0 kg N $ha^{-1}$ $yr^{-1}$ (12.6-57.1 μg N $m^{-2}$ $h^{-1}$), which is in good agreement with our measurements at Rambouillet where nitrogen deposition is enhanced by pollution arriving from Paris and other surrounding urbanized / industrialized areas. While noting that our fluxes are broadly consistent with previous measurements, we recognise that the calculations are based on the assumptions of a well-mixed boundary layer of fixed height arbitrarily set at 20 m and should not be over-interpreted.

### 4.3 Nitrogen Dioxide Losses

At nighttime, in the absence of its photolysis, $NO_2$ may be expected to increase in concentration (via R2) when a constant NO source exists (e.g. from soil, as observed here) and when $O_3$ is present. For both the Atlantic and the Continental phases an average diel profile between 20.00 and 04.00 UTC of $NO_2$ (black) is plotted in Figure 7. No obvious increase in $NO_2$ can be observed in the Atlantic phase and an average increase of around 1 ppbv can be observed in the Continental phase. The expected $NO_2$ resulting from the NO + $O_3$ reaction if there were no loss mechanisms of $NO_2$ is plotted in red. This is determined using the $NO_2$ measured at 20.00 UTC and incrementing this value by the $NO_2$ that would have been produced through NO oxidation by $O_3$ and peroxy radicals in each time step. In both phases, the simple assumption of nighttime $NO_2$ production through NO + $O_3$ and NO + $XO_2$ and no $NO_2$ loss results in significant generation of $NO_2$ with an overestimation of 10-12 ppbv of $NO_2$ at the end of the night compared to the measured $NO_2$. A loss mechanism of around 1.4 ppbv $h^{-1}$ of $NO_2$ is therefore necessary to explain the observed (lack of increase in) $NO_2$.

#### 4.3.1 Chemical Losses

While during the daytime $NO_2$ is removed in a largely irreversible process through reaction with OH radicals to form $HNO_3$, this is unlikely to represent a significant sink at nighttime. In the absence of photochemical formation pathways, OH is generated at night in the ozonolysis of olefins and in the reaction of $HO_2$ with $NO_3$ and NO.

$O_3$ + >=< $\rightarrow$ $\rightarrow$ OH (R11)

$NO_3 + HO_2 \rightarrow OH + NO_2 + O_2$ (R12)

$NO + HO_2 \rightarrow OH + NO_2$ (R4)

In the forested environment in summer, the emissions of biogenic volatile organic compounds (BVOC) (e.g. olefinic terpenoids) will favour R11 and simultaneously disfavour R12 as $NO_3$ will be reduced in concentration through its reactions with BVOCs. During the ACROSS campaign

ground $NO_3$ levels were generally below instrument detection limits of 2 pptv and we can reasonably ignore R12. Measurements of OH in forested environments are sparse, though they indicate that nocturnal OH levels are low, with concentrations generally lower than $1 \times 10^5$ molecule $cm^{-3}$. Combining the rate coefficient for reaction of OH with $NO_2$ of $\sim 1 \times 10^{-11}$ $cm^3$ $molecule^{-1}$ $s^{-1}$ (IUPAC, 2024) at ambient pressure and ≈ 300 K with an upper limit (confirmed by measurements) to the OH concentration of $1 \times 10^6$ molecule $cm^{-3}$ results in a $NO_2$ loss constant of $1 \times 10^{-5}$ $s^{-1}$, or (at the average nighttime $NO_2$ = 1650 pptv) a loss rate of ~60 ppt $h^{-1}$, clearly insufficient to explain the observations.

$NO_2$ is also lost via its reaction with $O_3$ to form the $NO_3$ radical (R8). In an upcoming paper, we will show that the majority of $NO_3$ formed in the forest will react with BVOCs rather than with NO (to re-form $NO_2$) and, to a good approximation, R8 represents an irreversible loss of $NO_2$ as the alkyl nitrates will not release nitrogen in the form of $NO_2$ at nighttime. However, the rate coefficient for this process ($3.5 \times 10^{-17}$ $cm^3$ $molecule^{-1}$ $s^{-1}$ at 298 K, (IUPAC, 2024)) is very small and with average nighttime $O_3$ levels reduced by deposition (see above) to 23 ppbv, the lifetime of $NO_2$ with respect to this reaction is 14 hours and the loss-rate (at the average nighttime $NO_2$ = 1650 pptv) is ~120 pptv $h^{-1}$, again too slow to contribute significantly to the apparent loss rate of $NO_2$.

The chemical loss of $NO_2$ via reaction with OH or via formation of $NO_3$ and its further reactions with BVOC to form alkyl nitrates is expected to result in the conversion of $NO_{\underline{x}}$ to $NO_{\underline{y}}$. As described in section 3.1.1, during the ACROSS campaign we operated a $NO_{\underline{y}}$ instrument to measure $NO_{\underline{y}}$ both in the gas- and particle-phases. Figure 8 displays the average diel profiles of $NO_{\underline{z}}$ ($NO_{\underline{y}}$-$NO_{\underline{x}}$) and $pNO_3$ during the Atlantic and Continental phases. For both $NO_{\underline{z}}$ and $pNO_3$ the diel profiles show either a decrease or stable mixing ratio across the period in which losses of 10-12 ppbv of $NO_2$ are required to explain the observations. Clearly, the loss of $NO_2$ at nighttime is not balanced by the formation of other forms of reactive nitrogen that were long lived enough to be detected. Trace gases such as $HNO_3$ or alkyl nitrates may be lost via deposition to surfaces, especially at high relative humidity and lifetimes for biogenic alkyl nitrates of a few hours have been reported (Liebmann et al., 2019; Farmer and Cohen, 2008; Browne et al., 2013; Romer Present et al., 2019). However, as shown above, the limiting step in the formation of organic nitrates is the slow reaction of $NO_2$ with $O_3$, which will not convert sufficient $NO_2$ to $NO_{\underline{z}}$ to explain our observations. Formation of organic nitrates that do not require the intermediacy of $NO_3$ (i.e. peroxy nitrates formed from $RO_2$ + $NO_2$) would also have been detected by the $NO_{\underline{y}}$ instrument and can thus also be ruled out as major reservoirs of $NO_{\underline{x}}$.

$NO_2$ deposited to humid surfaces can be converted to HONO and released to the atmosphere (Elshorbany et al., 2012; Meusel et al., 2016). A time series of HONO can be found in Figure S2 which reveals increases in HONO at nighttime. However, the HONO mixing ratios can account for only a small fraction of the $NO_2$ loss described above. This may reflect the fact that, if formed at a moist surface, (soluble) HONO is unlikely to desorb quantitatively into the gas-phase. The low HONO mixing ratios measured during the Atlantic phase compared to the Continental phase, could potentially be explained by the difference in soil humidity, however, the factors influencing

the formation and release of HONO are complex. The HONO observations will be analysed in detail in a seperate publication from the ACROSS campaign.

In the absence of other known gas-phase mechanisms for the removal of $NO_2$ at night and the fact that very little other reactive nitrogen trace-gases or nitrate particles are formed during the night, we conclude that physical removal of $NO_2$ (i.e. deposition) is responsible for its lack of build-up at night during ACROSS and that any transformation of $NO_2$ at the surface does not lead to quantitative release into the gas-phase

### 4.3.2 Physical Losses

$NO_2$ is known to be lost through dry deposition to surfaces such as soil and leaves, the latter depending on whether the stomata are open (daytime) or not fully open (nighttime) (Delaria et al., 2020; Delaria et al., 2018; Chaparro-Suarez et al., 2011). As for $O_3$, dry deposition of $NO_2$ to surfaces can be described by an exponential decay with a first-order decay rate constant, $k_L(NO_2) = (V_d/h)$, where $V_d$ is the deposition velocity and $h$ is the boundary layer height. This expression applies when gradients within the boundary layer are weak, as expected for $NO_2$ (see above) even though vertical mixing is very slow at night. The net production (or loss) of $NO_2$ is given by Eq. (2) where the first term on the right-hand side is the $NO_2$ production rate from the reaction of NO with $O_3$ or $XO_2$ (which is identical to the NO soil emission rate) and the second term is the loss rate assuming only depositional losses (see above) and ignoring entrainment of $NO_2$ from other heights. This will give an upper limit of the $NO_2$ deposition rate as a small fraction (<10%) of $NO_2$ is lost through chemical reactions with $O_3$ and OH (see above).

$$\frac{d[NO_2]}{dt} = E_{NO} - k_L(NO_2)[NO_2]_0 \quad (2)$$

$[NO_2]_0$ is the $NO_2$ mixing ratio at 20.00 UTC. The $NO_2$ concentration at any subsequent time can then be calculated as described in Eq. (3) with variation of $k_L(NO_2)$ in order to match the observed $NO_2$ mixing ratio.

$$[NO_2]_t = \int_0^t \frac{d[NO_2]}{dt} + [NO_2]_0 \quad (3)$$

In Figure 7 the grey lines symbolize the calculated $NO_2$ mixing ratios at nighttime using values of $k_L(NO_2)$ between $1.0 \times 10^{-4}$ and $4.0 \times 10^{-4}$ $s^{-1}$. As expected, no single value of $k_L(NO_2)$ can explain all the measurements as the height of the BL will not be invariant during the whole night. However, for the Continental and Atlantic phases the observed $NO_2$ can be explained with $k_L(NO_2) = (2.0 \pm 1.0) \times 10^{-4}$ $s^{-1}$ and $k_L(NO_2) = (2.75 \pm 1.25) \times 10^{-4}$ $s^{-1}$, respectively, which results in lifetimes of ~ 1-3 h and ~ 40-110 min for $NO_2$ at nighttime. As deposition of $NO_2$ in this environment represents a permanent loss of $NO_{x\underline{X}}$ from the gas phase, this lifetime can be compared to e.g. the lifetime of $NO_{x\underline{X}}$ with respect to its conversion to $HNO_3$ via reaction of $NO_2$ with OH which is ~ 1 day (assuming average $[OH] = 1 \times 10^6$ molecule $cm^{-3}$). The low aerosol surface area during ACROSS combined with the low uptake coefficient for $NO_2$ renders losses due to heterogeneous processes

insignificant (IUPAC, 2024). Clearly, only depositional losses of $NO_2$ in a forested environment contribute substantially to its lifetime at night and to the $NO_{x}$ budget.

If we continue to assume the nocturnal boundary layer at the forest site is at the top of the canopy (20 m), then the $NO_2$ loss-rate constants we determined can be converted to a deposition velocity of 0.4 ± 0.2 cm $s^{-1}$ and 0.55 ± 0.25 cm $s^{-1}$ for the Continental and Atlantic phase, respectively. These are comparable to previous measurements of $NO_2$ deposition velocities of 0.15 cm $s^{-1}$ (Dewald et al., 2022), 0.1-0.57 cm $s^{-1}$ (Rondón et al., 1993), 0.098 cm $s^{-1}$ (Breuninger et al., 2013), 0.2-0.5 cm $s^{-1}$ (Horii et al., 2004), 0.02-0.64 cm $s^{-1}$ (Puxbaum and Gregori, 1998), for a mountain observatory surrounded by coniferous trees, boreal coniferous forests, a temperate coniferous forest, a temperate mixed deciduous forest, and a temperate oak forest, respectively, where a combination of soil and foliage deposition is measured. Horii et al. (2004) saw an increase in deposition velocity with increasing $NO_2$ mixing ratio; from 0.2 cm $s^{-1}$ at 1 ppbv to 0.5 cm $s^{-1}$ at 30 ppbv. Puxbaum and Gregori (1998) reported monthly averages of 0.02-0.64 cm $s^{-1}$, however, their nighttime deposition velocities averaged below 0.05 cm $s^{-1}$. The deposition velocities determined here are a factor of 5-40 higher than what has been measured for nighttime foliage deposition velocities to the leaves of different trees native to California (Delaria et al., 2020; Delaria et al., 2018), but in good agreement with measurements for daytime. It is, however, important to note that the deposition velocities estimated here are upper limits as the estimation of the NO emission rate is an upper limit and chemical loss of $NO_2$ is not taken into account. Using an average nighttime $NO_2$ mixing ratio of 1650 and 1450 pptv for the Continental and Atlantic phase, respectively, results in $NO_2$ deposition rates of 13.6 ± 6.8 μg N $m^{-2}$ $h^{-1}$ and 18.7 ± 8.5 μg N $m^{-2}$ $h^{-1}$, which are in reasonable agreement with that measured for soil $NO_2$ deposition in a sessile oak forest of 9.67 ± 1.92 μg N $m^{-2}$ $h^{-1}$ during the summer (Rosenkranz et al., 2006). The estimated NO soil emission rate and $NO_2$ deposition rate are, within the uncertainties, identical, which means the Rambouillet forest is not a significant direct source or sink of $NO_{x}$.

## 5 ~~Summary~~Conclusions:

Measurements of NO, $NO_2$, $NO_{y}$, and $O_3$ during the ACROSS campaign (June-July 2022) in the Rambouillet forest southwest of Paris, France, have been used to gain insight into nighttime processes controlling $NO_{x}$ in an anthropogenically impacted forest environment. Based on HYSPLIT back trajectories, two phases of the campaign were identified; one dominated by air originating over the Atlantic Ocean ("Atlantic"), which on average had high relative humidity and low $O_3$ mixing ratios, and one dominated by continental air masses from different urban/industrialized regions ("Continental"), which on average had a lower relative humidity than the Atlantic phase and higher $O_3$ mixing ratios. Strong diel profiles were observed in the $O_3$ measurements across the campaign with daytime peak mixing ratios varying from ~30 to 90 ppbv and nighttime tending towards 0-10 ppbv. The daily variation was driven by a variable but generally rapid $O_3$ deposition to soil and foliar surfaces, with a strong influence of relative humidity (influencing the surface resistance to uptake) and inversion (influencing the rate of entrainment of $O_3$ from above the canopy).

During the Atlantic phase, periods of sustained NO above the instrumental detection limit was observed at nighttime when $O_3$ was sufficiently low (i.e. the NO lifetime sufficiently long). This enabled the derivation of an average NO emission rate from the soil ($E_{NO}$) of ~1.4 ppbv $h^{-1}$, which was confirmed by the approximately linear increase in NO observed in the absence of $O_3$ in the Atlantic phase. The estimated $E_{NO}$ is in broad agreement with previous measurements in other European temperate forests with tree types as found in the Rambouillet forest. The uncertainty in the estimated NO emission rate is determined from the uncertainties in NO and $O_3$ at 3-5 m above ground, which leads to higher relative uncertainties at low NO and $O_3$ mixing ratios. Measurements of either NO fluxes or highly resolved height profiles of NO and $O_3$ will improve the NO emission rate estimate during future field campaigns.

An increase in $NO_2$ at night would be expected when having a constant NO emission rate of ~1.4 ppbv $h^{-1}$ in the presence of $O_3$ as observed in this study, however, this was not the case. The lack of increase in $NO_2$ was used to estimate first-order decay constants of $(2.0 \pm 1.0) \times 10^{-4}$ $s^{-1}$ and $(2.75 \pm 1.25) \times 10^{-4}$ $s^{-1}$ resulting in an effective lifetime of $NO_2$ of ~0.5-3 h. The loss of $NO_2$ at nighttime is presumably driven by deposition to soil and foliar surfaces since the lifetime of $NO_2$ towards its reactions with OH and $O_3$ at night is >28 and 14 h, respectively. By comparison, the daytime lifetime of $NO_2$ with respect to loss by reaction with OH is about 1 day. We conclude that the nighttime deposition of $NO_2$ is a major sink of boundary layer $NO_{x}$ in this forested environment.

## 6 Data Availability:

All data can be found on https://across.aeris-data.fr/catalogue/.

## 7 Author contribution:

All authors contributed with measurements. Data analysis was conducted by STA with contributions from JNC and PD. CC and VM organized the field campaign with contributions from the individual group leads. STA and JNC developed the manuscript with contributions from all authors.

## 8 Competing Interests:

At least one of the (co-)authors is a member of the editorial board of Atmospheric Chemistry and Physics

## 9 Acknowledgements:

STA is thankful to the Alexander von Humboldt foundation for funding her stay at MPIC.

PD gratefully acknowledges the Deutsche Forschungsgemeinschaft (project “MONOTONS”, project number: 522970430).

The ACROSS project has received funding from the French National Research Agency (ANR) under the investment program integrated into France 2030, with the reference ANR-17-MPGA-0002, and it was supported by the French National program LEFE (Les Enveloppes Fluides et l'Environnement) of the CNRS/INSU (Centre National de la Recherche Scientifique/Institut National des Sciences de l'Univers). Data from the ACROSS campaign are hosted by the French national center for Atmospheric data and services AERIS.

IMT Nord Europe acknowledges financial support from the CaPPA project, which is funded by the French National Research Agency (ANR) through the PIA (Programme d’Investissement d’Avenir) under contract ANR-11-LABX-0005-01, the Regional Council “Hauts-de-France” and the European Regional Development Fund (ERDF).

## 10 References:

Altimir, N., et al.: Foliage surface ozone deposition: a role for surface moisture?, Biogeosciences, 3, 209-228, 10.5194/bg-3-209-2006, 2006.

Breuninger, C., et al.: Field investigations of nitrogen dioxide (NO<sub>2</sub>) exchange between plants and the atmosphere, Atmos. Chem. Phys., 13, 773-790, 10.5194/acp-13-773-2013, 2013.

Browne, E. C., et al.: Observations of total $RONO_2$ over the boreal forest: NO*x* sinks and $HNO_3$ sources, Atmospheric Chemistry and Physics, 13, 4543-4562, 10.5194/acp-13-4543-2013, 2013.

Burkhardt, J. and Eiden, R.: Thin water films on coniferous needles: A new device for the study of water vapour condensation and gaseous deposition to plant surfaces and particle samples, Atmospheric Environment, 28, 2001-2011, https://doi.org/10.1016/1352-2310(94)90469-3, 1994.

Cantrell, C. and Michoud, V.: An Experiment to Study Atmospheric Oxidation Chemistry and Physics of Mixed Anthropogenic–Biogenic Air Masses in the Greater Paris Area, Bulletin of the American Meteorological Society, 103, 599-603, https://doi.org/10.1175/BAMS-D-21-0115.1, 2022.

Chaparro-Suarez, I. G., et al.: Nitrogen dioxide (NO2) uptake by vegetation controlled by atmospheric concentrations and plant stomatal aperture, Atmospheric Environment, 45, 5742-5750, https://doi.org/10.1016/j.atmosenv.2011.07.021, 2011.

Ciencewicki, J. and Jaspers, I.: Air Pollution and Respiratory Viral Infection, Inhalation Toxicology, 19, 1135-1146, 10.1080/08958370701665434, 2007.

Davidson, E. A. and Kingerlee, W.: A global inventory of nitric oxide emissions from soils, Nutrient Cycling in Agroecosystems, 48, 37-50, 10.1023/A:1009738715891, 1997.

Delaria, E. R. and Cohen, R. C.: A model-based analysis of foliar NOx deposition, Atmos. Chem. Phys., 20, 2123-2141, 10.5194/acp-20-2123-2020, 2020.

Delaria, E. R., et al.: Laboratory measurements of stomatal NO2 deposition to native California trees and the role of forests in the NOx cycle, Atmos. Chem. Phys., 20, 14023-14041, 10.5194/acp-20-14023-2020, 2020.

607 Delaria, E. R., et al.: Measurements of NO and $NO_2$ exchange between the atmosphere and
608 Quercus agrifolia, Atmos. Chem. Phys., 18, 14161-14173, 10.5194/acp-18-14161-2018, 2018.
609 Dewald, P., et al.: Fate of the nitrate radical at the summit of a semi-rural mountain site in Germany
610 assessed with direct reactivity measurements, Atmos. Chem. Phys., 22, 7051-7069,
611 10.5194/acp-22-7051-2022, 2022.
612 Draxler, R. R. and Rolph, G. D.: HYSPLIT (HYbrid Single-Particle Lagrangian Integrated
613 Trajectory) Model access via NOAA ARL READY Website
614 (http://ready.arl.noaa.gov/HYSPLIT.php). NOAA Air Resources Laboratory, Silver Spring,
615 MD., 2011.
616 Elshorbany, Y. F., et al.: Impact of HONO on global atmospheric chemistry calculated with an
617 empirical parameterization in the EMAC model, Atmos. Chem. Phys., 12, 9977-10000,
618 10.5194/acp-12-9977-2012, 2012.
619 Emberson, L. D., et al.: Ozone effects on crops and consideration in crop models, European Journal
620 of Agronomy, 100, 19-34, https://doi.org/10.1016/j.eja.2018.06.002, 2018.
621 Farmer, D. K. and Cohen, R. C.: Observations of $HNO_3$, ΣAN, ΣPN and $NO_2$ fluxes: evidence for
622 rapid $HO_x$ chemistry within a pine forest canopy, Atmos. Chem. Phys., 8, 3899-3917,
623 10.5194/acp-8-3899-2008, 2008.
624 Finkelstein, P. L., et al.: Ozone and sulfur dioxide dry deposition to forests: Observations and
625 model evaluation, Journal of Geophysical Research: Atmospheres, 105, 15365-15377,
626 https://doi.org/10.1029/2000JD900185, 2000.
627 Friedrich, N., et al.: Measurement of NOx and NOy with a thermal dissociation cavity ring-down
628 spectrometer (TD-CRDS): instrument characterisation and first deployment, Atmos. Meas.
629 Tech., 13, 5739-5761, 10.5194/amt-13-5739-2020, 2020.
630 Ganzeveld, L. and Lelieveld, J.: Dry deposition parameterization in a chemistry general circulation
631 model and its influence on the distribution of reactive trace gases, Journal of Geophysical
632 Research: Atmospheres, 100, 20999-21012, https://doi.org/10.1029/95JD02266, 1995.
633 Gessler, A., et al.: NH3 and NO2 fluxes between beech trees and the atmosphere – correlation with
634 climatic and physiological parameters, New Phytologist, 147, 539-560,
635 https://doi.org/10.1046/j.1469-8137.2000.00712.x, 2000.
636 Geyer, A. and Stutz, J.: Vertical profiles of $NO_3$, $N_2O_5$, $O_3$, and NO*x* in the nocturnal boundary
637 layer: 2. Model studies on the altitude dependence of composition and chemistry (vol 109, art
638 no D16399, 2004), Journal of Geophysical Research-Atmospheres, 109,
639 10.1029/2004JD005217 2004.
640 Hallquist, M., et al.: The formation, properties and impact of secondary organic aerosol: current
641 and emerging issues, Atmospheric Chemistry and Physics, 9, 5155-5236, 10.5194/acp-9-5155-
642 2009, 2009.
643 Heland, J., et al.: A new instrument to measure gaseous nitrous acid (HONO) in the atmosphere,
644 Environmental Science & Technology, 35, 3207-3212, DOI 10.1021/es000303t, 2001.
645 Hens, K., et al.: Observation and modelling of HOx radicals in a boreal forest, Atmospheric
646 Chemistry and Physics, 14, 8723-8747, 10.5194/acp-14-8723-2014, 2014.
647 Horii, C. V., et al.: Fluxes of nitrogen oxides over a temperate deciduous forest, Journal of
648 Geophysical Research: Atmospheres, 109, https://doi.org/10.1029/2003JD004326, 2004.
649 IUPAC Task Group on Atmospheric Chemical Kinetic Data Evaluation, (Ammann, M., Cox, R.A.,
650 Crowley, J.N., Herrmann, H., Jenkin, M.E., McNeill, V.F., Mellouki, A., Rossi, M. J., Troe, J.
651 and Wallington, T. J.). Last access April. 2024: https://iupac.aeris-data.fr/, last

Jaeglé, L., et al.: Global partitioning of NOx sources using satellite observations: Relative roles of fossil fuel combustion, biomass burning and soil emissions, Faraday Discussions, 130, 407-423, 10.1039/B502128F, 2005.
Kanakidou, M., et al.: Organic aerosol and global climate modelling: a review, Atmospheric Chemistry and Physics, 5, 1053-1123, 10.5194/acp-5-1053-2005, 2005.
Kane, S. M., et al.: Heterogeneous uptake of gaseous $N_2O_5$ by $(NH_4)_2SO4$, $NH_4HSO_4$, and $H_2SO_4$ aerosols, Journal of Physical Chemistry a, 105, 6465-6470, 2001.
Kiendler-Scharr, A., et al.: Ubiquity of organic nitrates from nighttime chemistry in the European submicron aerosol, Geophysical Research Letters, 43, 7735-7744, 10.1002/2016gl069239, 2016.
Kleffmann, J., et al.: Intercomparison of the DOAS and LOPAP techniques for the detection of nitrous acid (HONO), Atmospheric Environment, 40, 3640-3652, https://doi.org/10.1016/j.atmosenv.2006.03.027, 2006.
Kukui, A., et al.: Chemical ionisation mass spectrometer for measurements of OH and Peroxy radical concentrations in moderately polluted atmospheres, Journal of Atmospheric Chemistry, 61, 133-154, 10.1007/s10874-009-9130-9, 2008.
Kurpius, M. R. and Goldstein, A. H.: Gas-phase chemistry dominates $O_3$ loss to a forest, implying a source of aerosols and hydroxyl radicals to the atmosphere, Geophysical Research Letters, 30, 10.1029/2002gl016785, 2003.
Liebmann, J., et al.: Alkyl nitrates in the boreal forest: formation via the NO3-, OH- and O3-induced oxidation of biogenic volatile organic compounds and ambient lifetimes, Atmos. Chem. Phys., 19, 10391-10403, 10.5194/acp-19-10391-2019, 2019.
Liebmann, J. M., et al.: Direct measurements of NO3 reactivity in and above the boundary layer of a mountaintop site: identification of reactive trace gases and comparison with OH reactivity, Atmospheric Chemistry and Physics, 18, 12045-12059, 10.5194/acp-18-12045-2018, 2018.
Lightfoot, P. D., et al.: Organic peroxy radicals - kinetics, spectroscopy and tropospheric chemistry, Atmospheric Environment, Part A: General Topics, 26, 1805-1961, 1992.
Meusel, H., et al.: Daytime formation of nitrous acid at a coastal remote site in Cyprus indicating a common ground source of atmospheric HONO and NO, Atmospheric Chemistry and Physics, 16, 14475-14493, 10.5194/acp-16-14475-2016, 2016.
Padro, J.: Seasonal contrasts in modelled and observed dry deposition velocities of O3, SO2 and NO2 over three surfaces, Atmospheric Environment. Part A. General Topics, 27, 807-814, https://doi.org/10.1016/0960-1686(93)90002-G, 1993.
Padro, J.: Summary of ozone dry deposition velocity measurements and model estimates over vineyard, cotton, grass and deciduous forest in summer, Atmospheric Environment, 30, 2363-2369, https://doi.org/10.1016/1352-2310(95)00352-5, 1996.
Phillips, G. J., et al.: The detection of nocturnal $N_2O_5$ as $HNO_3$ by alkali- and aqueous-denuder techniques, Atmospheric measurement techniques, 6, 231-237, 10.5194/amt-6-231-2013, 2013.
Phillips, G. J., et al.: Significant concentrations of nitryl chloride observed in rural continental Europe associated with the influence of sea salt chloride and anthropogenic emissions, Geophysical Research Letters, 39, L10811, doi:10.1029/2012GL051912, 2012.
Pilegaard, K.: Processes regulating nitric oxide emissions from soils, Philosophical Transactions of the Royal Society B-Biological Sciences, 368, ARTN 20130126
10.1098/rstb.2013.0126, 2013.

Pilegaard, K., et al.: Factors controlling regional differences in forest soil emission of nitrogen oxides (NO and N<sub>2</sub>O), Biogeosciences, 3, 651-661, 10.5194/bg-3-651-2006, 2006.
Puxbaum, H. and Gregori, M.: Seasonal and annual deposition rates of sulphur, nitrogen and chloride species to an oak forest in north-eastern austria (wolkersdorf, 240 m a.s.l.), Atmos. Env., 32, 3557-3568, https://doi.org/10.1016/S1352-2310(98)00073-9, 1998.
Rannik, Ü., et al.: Ozone deposition into a boreal forest over a decade of observations: evaluating deposition partitioning and driving variables, Atmos. Chem. Phys., 12, 12165-12182, 10.5194/acp-12-12165-2012, 2012.
Romer Present, P. S., et al.: The changing role of organic nitrates in the removal and transport of NOx, Atmos. Chem. Phys. Discuss., 2019, 1-18, 10.5194/acp-2019-471, 2019.
Rondón, A., et al.: Dry deposition of nitrogen dioxide and ozone to coniferous forests, Journal of Geophysical Research: Atmospheres, 98, 5159-5172, https://doi.org/10.1029/92JD02335, 1993.
Rosenkranz, P., et al.: Soil N and C trace gas fluxes and microbial soil N turnover in a sessile oak (Quercus petraea (Matt.) Liebl.) forest in Hungary, Plant and Soil, 286, 301-322, 10.1007/s11104-006-9045-z, 2006.
Schindlbacher, A., et al.: Effects of soil moisture and temperature on NO, NO2, and N2O emissions from European forest soils, Journal of Geophysical Research: Atmospheres, 109, https://doi.org/10.1029/2004JD004590, 2004.
Schumann, U. and Huntrieser, H.: The global lightning-induced nitrogen oxides source, Atmos. Chem. Phys., 7, 3823-3907, 10.5194/acp-7-3823-2007, 2007.
Shepson, P. B., et al.: Determination of the relative ozone and PAN deposition velocities at night, Geophysical Research Letters, 19, 1121-1124, 10.1029/92gl01118, 1992.
Sobanski, N., et al.: A five-channel cavity ring-down spectrometer for the detection of $NO_2$, $NO_3$, $N_2O_5$, total peroxy nitrates and total alkyl nitrates, Atmospheric Measurement Techniques, 9, 5103-5118, 10.5194/amt-9-5103-2016, 2016.
Stutz, J., et al.: Vertical profiles of $NO_3$, $N_2O_5$, $O_3$, and $NO_X$ in the nocturnal boundary layer: 1. Observations during the Texas Air Quality Study 2000 Journal of Geophysical Research-Atmospheres, 109, art. D12306, 10.1029/2003JD004209, 2004.
Thoene, B., et al.: Absorption of atmospheric NO2 by spruce (Picea abies) trees, New Phytologist, 134, 257-266, https://doi.org/10.1111/j.1469-8137.1996.tb04630.x, 1996.
Val Martin, M., et al.: Large-scale impacts of anthropogenic pollution and boreal wildfires on the nitrogen oxides over the central North Atlantic region, Journal of Geophysical Research: Atmospheres, 113, https://doi.org/10.1029/2007JD009689, 2008.
Weber, P. and Rennenberg, H.: Dependency of nitrogen dioxide (NO2) fluxes to wheat (Triticum aestivum L.) leaves from NO2 concentration, light intensity, temperature and relative humidity determined from controlled dynamic chamber experiments, Atmospheric Environment, 30, 3001-3009, https://doi.org/10.1016/1352-2310(96)00008-8, 1996.
Wu, Z., et al.: Dry deposition of O3 and SO2 estimated from gradient measurements above a temperate mixed forest, Environmental Pollution, 210, 202-210, https://doi.org/10.1016/j.envpol.2015.11.052, 2016.
Zhou, P., et al.: Simulating ozone dry deposition at a boreal forest with a multi-layer canopy deposition model, Atmos. Chem. Phys., 17, 1361-1379, 10.5194/acp-17-1361-2017, 2017.

## 11 Figures:

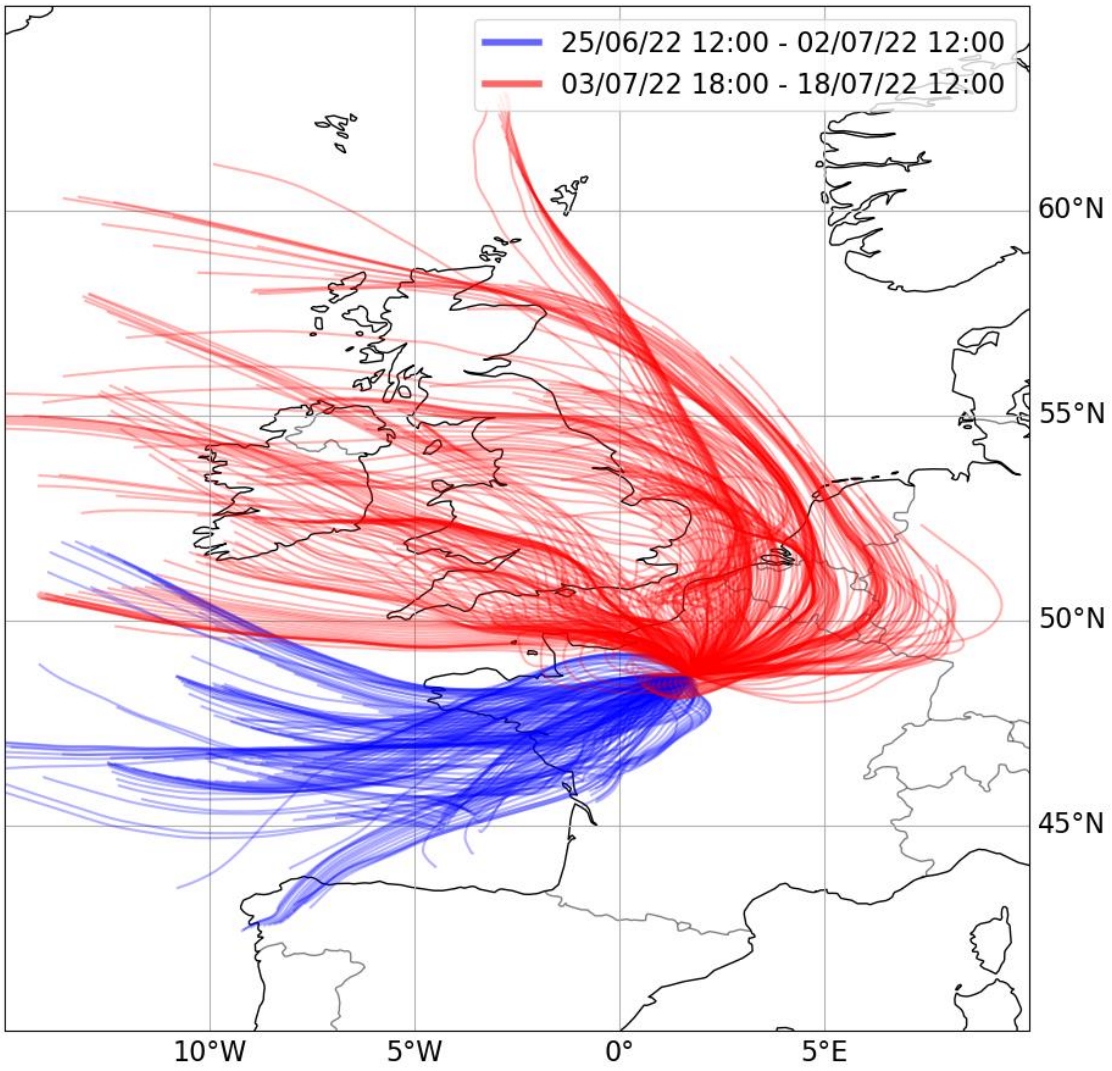


Figure 1: 48-hour back trajectories from the Rambouillet forest supersite using the Hybrid Single-Particle Lagrangian Integrated Trajectory model (HYSPLIT, version 4, 2019).

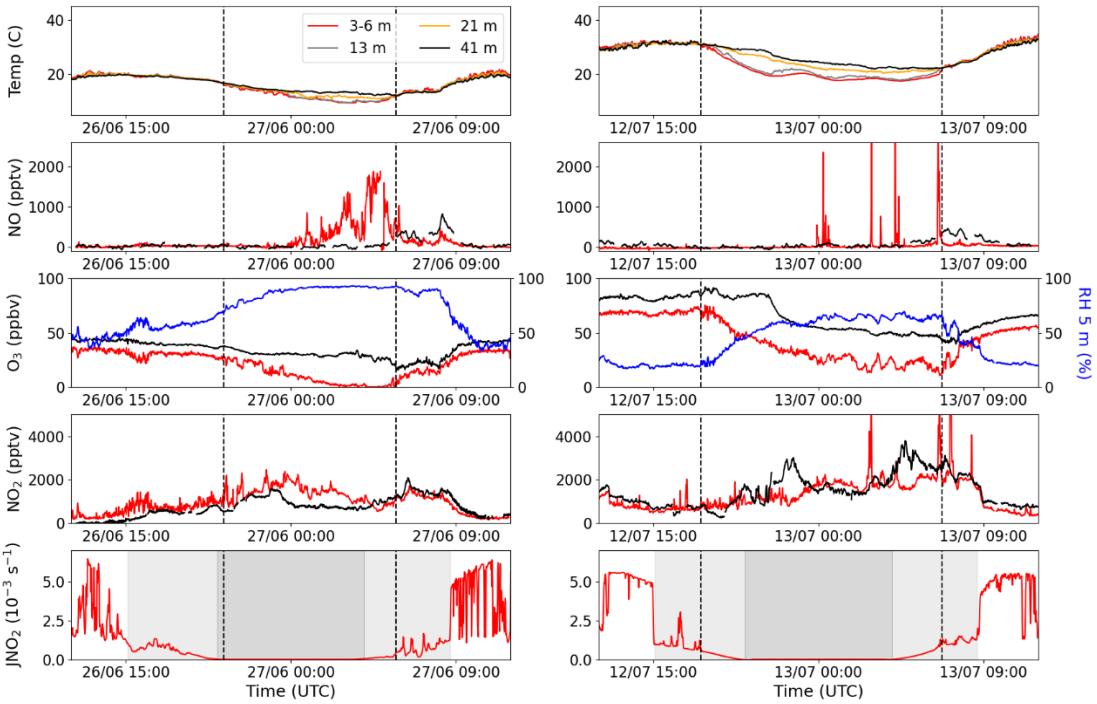


Figure 2: Measurements of temperature, NO, $O_3$, RH, $NO_2$, and $JNO_2$ for two different nights during the campaign; one during the Atlantic phase (left panels) and one during the continental phase (right panels). The different colours symbolize four different heights; red = 3-6 m, grey = 13 m, orange = 21 m, and black = 41 m, and the blue shows the RH at 5 m. The grey shaded areas in the $JNO_2$ plots shows the time the MPIC container was in shade during the afternoon and morning (light grey) and nighttime (dark grey). The vertical black dashed lines indicate the beginning and end of the observed temperature inversions in the top panels.

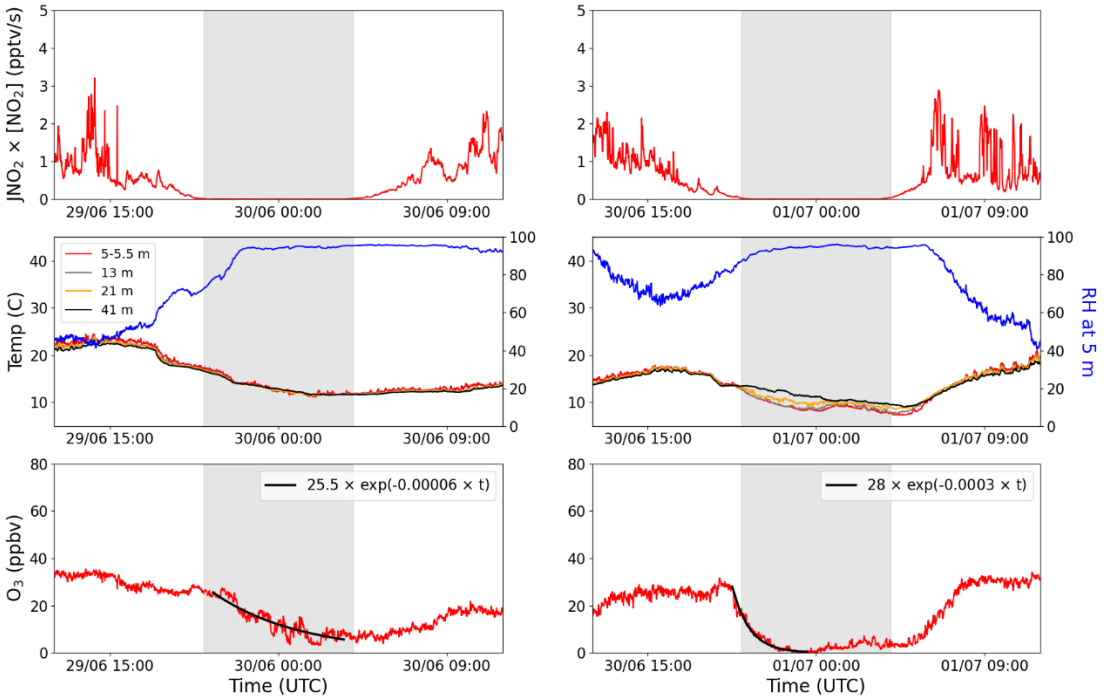


Figure 3: The production of $O_3$ ($JNO_2 \times [NO_2]$), temperature, RH, and $O_3$ plotted for two nights with high average RH; one without a temperature inversion (left panels) and one with a temperature inversion (right panels). The different colours symbolize four different heights; red = 5-5.4 m, grey = 13 m, orange = 21 m, and black = 41 m, and the blue shows the RH at 5 m. The net nighttime $O_3$ loss is fitted with an exponential decay curve (solid black line) in the bottom plots. The grey shaded areas represent the nighttime.

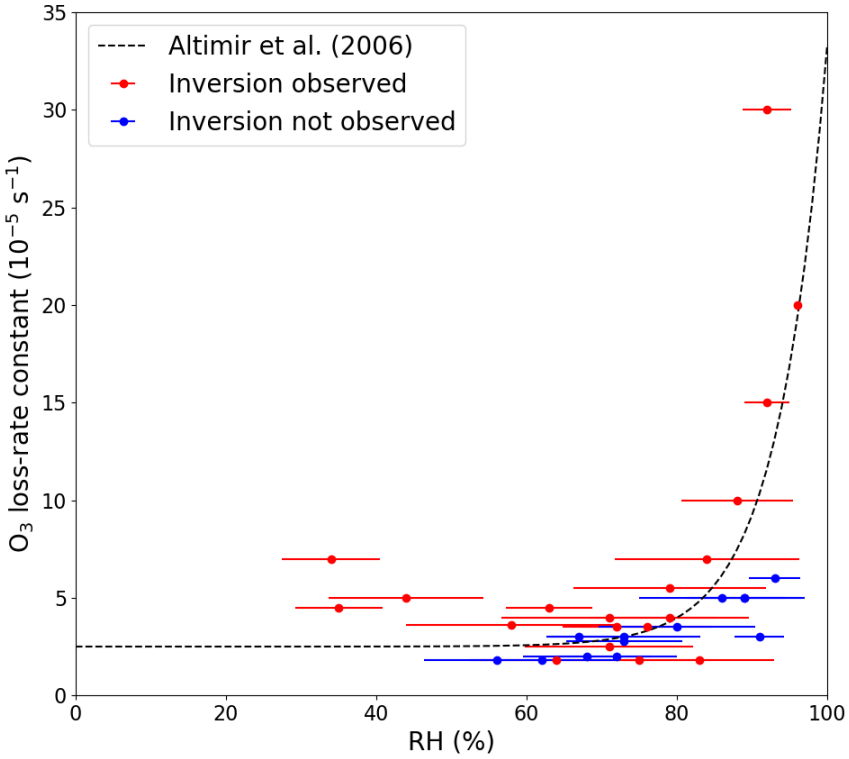


Figure 4: Net $O_3$ loss-rate constants at 5.4 m plotted against the average relative humidity measured during the time used to fit the exponential decay of $O_3$. The error bars represent ±1σ on the average RH. The dashed line symbolizes the observations made by Altimir et al. (2006).

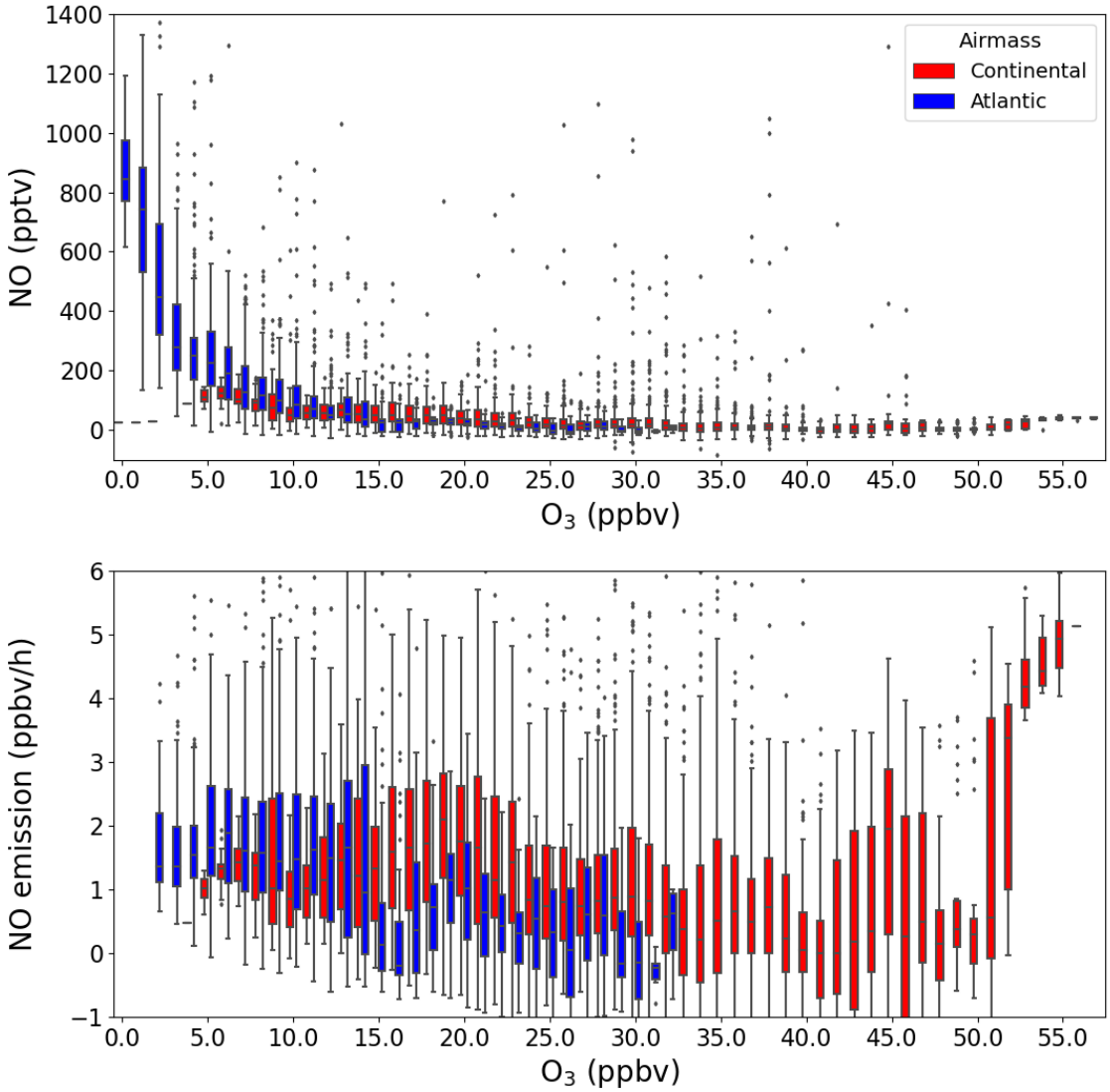


766

767 Figure 5: NO (top) and NO emission (bottom) plotted against $O_3$ in a box-and-whiskers plot, where
768 the outliers are defined as being outside 1.5 × IQR. The colours represent the two different air
769 masses.

770

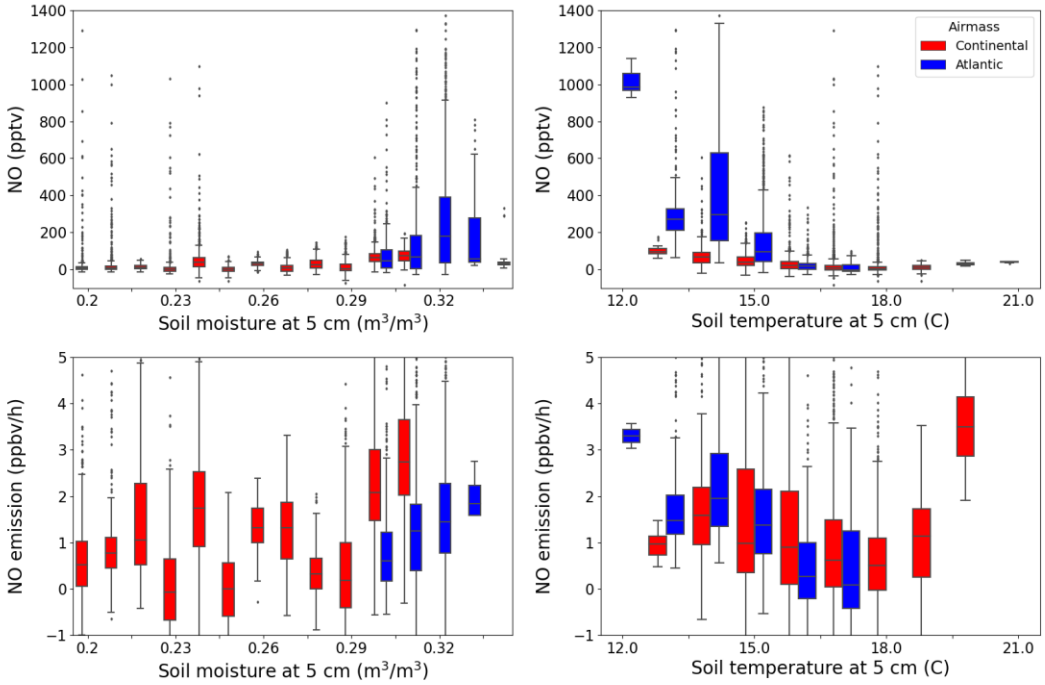


Figure 6: NO (top panels) and NO emission (bottom panels) plotted against soil moisture (left panels) and temperature (right panels) at 5 cm below the surface in a box-and-whiskers plot, where the outliers are defined as being outside 1.5 × IQR. The colours represent the two different air masses.

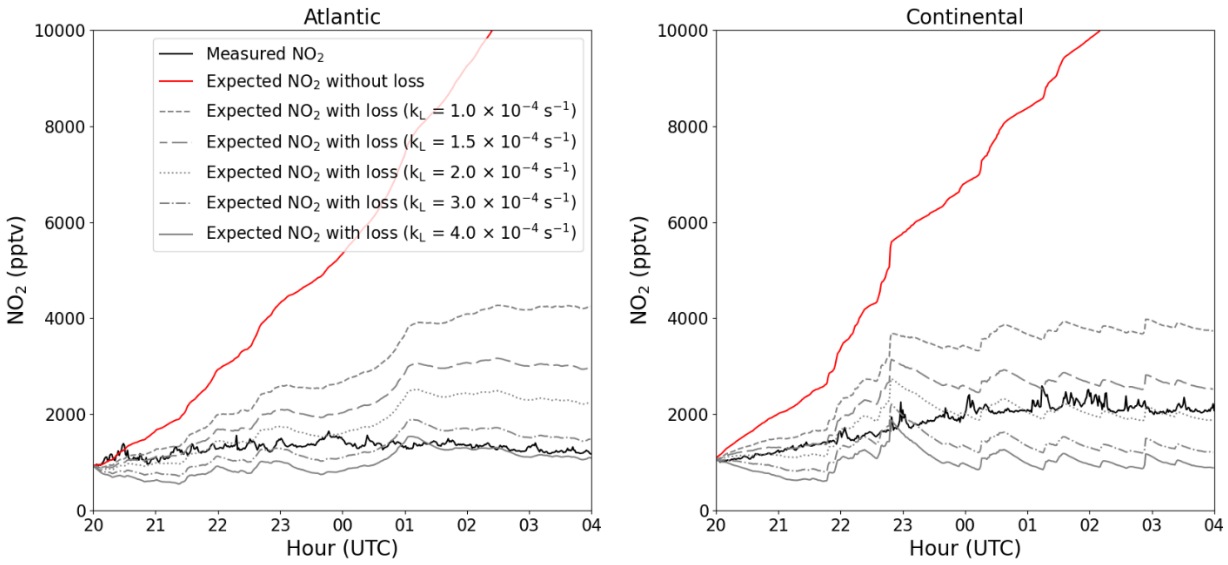


777

778 Figure 7: Average nighttime profiles of $NO_2$ at 5.4 m for each of the two phases (black) plotted
779 together with the expected $NO_2$ with (grey) and without (red) $NO_2$ loss.

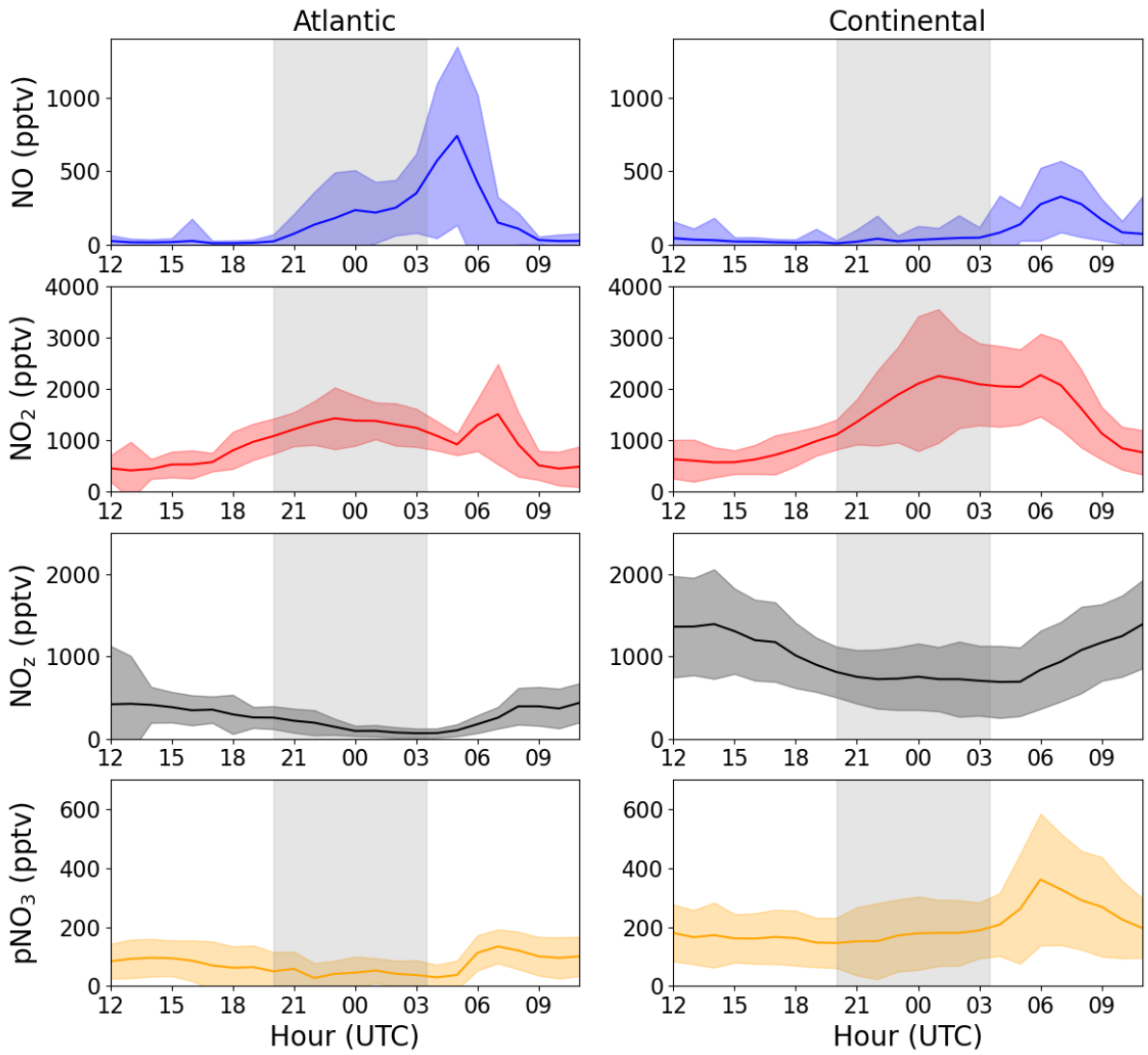


780

781 Figure 8: Average diel profiles of NO, $NO_2$, total gas-phase $NO_z$, and particulate nitrate ($pNO_3$) at
782 3-6 m above ground for the Atlantic (left panels) and Continental (right panels) phases. The grey
783 shaded areas symbolize nighttime.

## 12 Tables:

Table 1: Measured NO soil emission in European forests with the same tree types as in the Rambouillet forest.

| Dominant tree type | Location | NO emission ($\mu g\ N\ m^{-2}\ h^{-1}$) | Reference |
|---|---|---|---|
| Oak | Matra Mountains, Hungary | 2.1 | (Pilegaard et al., 2006) |
| | | 6.0 ± 3.3 (summer) | (Rosenkranz et al., 2006) |
| | | 8.4 ± 2.4 (autumn) | (Rosenkranz et al., 2006) |
| Pine | San Rossore, Italy | 5.4 | (Pilegaard et al., 2006) |
| Beech | Schottenwald, Austria | 25.5 ± 7.5 | (Schindlbacher et al., 2004) |
| | | 4.2 | (Pilegaard et al., 2006) |
| Beech | Klausen-Leopolsdorf, Austria | 10.2 ± 3.4 | (Schindlbacher et al., 2004) |
| | | 0.7 | (Pilegaard et al., 2006) |
| Spruce-Fir-Beech | Achenkirch, Austria | 2.8 ± 1.4 | (Schindlbacher et al., 2004) |
| | | 0.9 | (Pilegaard et al., 2006) |
| Mixed deciduous | Ticino Park, Italy | 18.5 ± 5.8 | (Schindlbacher et al., 2004) |
| | | Below LOD | (Pilegaard et al., 2006) |